N73-21279

NASA TECHNICAL TRANSLATION NASA TT F-14,881

PULSATING FLOW THROUGH PIPES

F. Schultz-Grunow

CASE FILE COPY

Translation of: "Pulsierender Durchfluss durch Rohre," Forschung, Vol. 11, No. 4, 1940, pp. 170-187.

NATIONAL AERONAUTICS AND SPACE ADMINISTRATION
WASHINGTON, D. C. 20546 APRIL 1973

PULSATING FLOW THROUGH PIPES

F. Schultz-Grunow*

Known experimental installations attempt to satisfy the practical requirement for measurement of the amount of liquid and an overall estimation of the pipe resistance in the case of pulsations [1,2]. They do not furnish information regarding the instantaneous flow and friction conditions of the turbulent friction layer for unsteady flow. The present paper*** therefore attempts to clarify these unknown processes. The same experimental installation is used as was found to be expedient for steady conditions. This is the experiment with a straight pipe through which the flow pulsates. We did not measure the prime average values using pressure measurement instruments having a large degree of damping. This is because we are not interested in instantaneous values and such stagnation pressure measurements result in average values which are not convenient for evaluation. Also the pressure decrease measurements result in an average value which cannot be used to estimate the friction resistance.

/170**

*Kaiser-Wilhelm-Institute of Flow Research, Gottingen

**Numbers in the margin indicate pagination in the foreign text.

***The research board for vehicular traffic and the association of German engineers (VDI) made funds available for this project. This paper is also being published in volume 48 of the series "German Vehicular Traffic Research", Berlin 1940.

1. EXPERIMENTAL INSTALLATION

The water flows from an expansion tank a (Figure 1), which is supplied by a water pump b, into the starting pipe c having the diameter of the experimental pipe. This is the normal industrial pipe and has a length of 112 times its diameter. In this way we avoid a possible rotation due to friction which could occur at the inlet. The experimental pipe d, which is connected with the starting pipe, has a highly polished brass pipe with a diameter of 50 mm and a length of 3.5 m. Nikuradse [3] already used this in his experiments. The preliminary experiments took far more time than the main experiments. Some calcium was deposited in this pipe because the water had a high calcium content. It was left in the pipe in order to avoid constant cleaning of the pipe during the experiments. The roughness of the pipe was found to be the same before and after the main experiments. This was shown by pressure drop measurements for steady flow. A box e is flanged to the pipe which contains the stagnation tubes with which the stagnation pressure profile at the pipe end cross section was measured. The rotational slide f which opens periodically is attached to the box. It produces a pulsating flow. The water then runs into the box. In this arrangement the pulsation is not positively controlled, because the inertia of the water column contained in the pipe can influence the course of the pulsation by reducing the pulsation amplitude as the frequency increases.

The rotational slide, the construction of which is shown in Figure 2, essentially consists of a hollow cylinder a installed in a housing. It has two diametrically opposing slots b in which a second well-fitted and hermetically sealed hollow cylinder c is turned by means of the rod d. The rod is then driven through a chain wheel e by an electrical motor. One end of the cylinder c is formed in such a way that its development

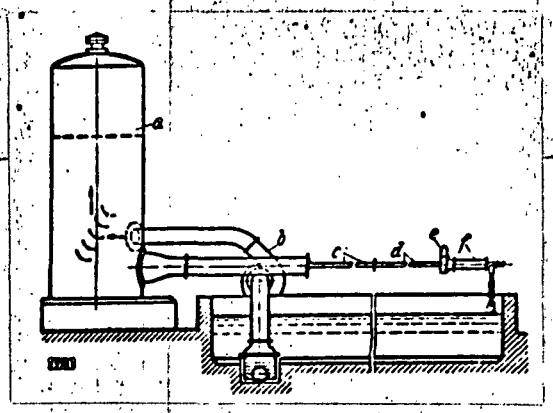

Figure 1. Experimental installation

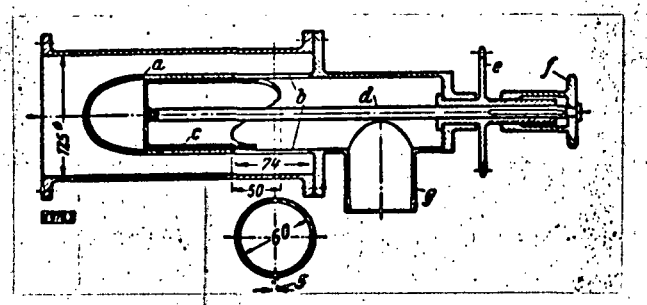

Figure 2. Rotary slide for producing pulsations.

results in a sinusoidal line of two periods. This end periodically opens the slots of the cylinder a when it moves. In addition to the periodic opening, there can be an axial displacement of the cylinder c using the handwheel f which results in a displacement called L later on. L is measured from a specified zero point. This produces a constant aperture cross section which remains constant during the rotation. The water flows through the slots b into the interior of the cylinder. From there it is removed through the outlet g. /171

The experiments were performed in the usual way. The pressure drop in the pipe was measured with holes in the wall and the velocity profile was measured at the end of the pipe using stagnation pipes. Under steady conditions, usually a single very fine stagnation pipe is used which slides along a diameter and uses rubber hoses. This could not be done here, because for pulsating pressures the pipe connections from the measurement points to the pressure measurement instruments must be rigid. Therefore a fixed arrangement of the measurement installation had to be produced. Consequently there are a number of stagnation pipes along the perpendicular pipe diameter in the box flanged to the pipe end. These are attached rigidly at a distance of 2.3 mm from the final pipe cross section. The stagnation pipe distances are shown in Figure 3. Most of the stagnation pipes are along the upper radius. The few stagnation pipes along the lower radius are used to test whether or not there is indeed a symetric velocity profile. The inner diameters of the stagnation probes are 0.6 mm and are quite large compared with the pipe diameter. Originally we installed even finer stagnation pipes having an interior diameter of 0.2 mm. However we found that the measurement technique using the stroboscopic valve, to be described later, required such a long adjustment time, that measurements with these fine stagnation pipes became impossible.

Stagnation pressure profiles and pressure drops are to be measured at various times during the pulsation. In order to be able to record the large required number of measurement points rapidly, a multiple manometer was set up, like the one used by the Aerodynamic Test Installation at Gottingen in wind tunnel measurements. Figure 4 shows that it consists of a number of pipes attached to a metal frame. There is a glass plate with an etched millimeter scale in front of the pipes. Behind the pipes there is an opaque glass plate through the manometer levels are illuminated with tungsten filament lamps. They can then

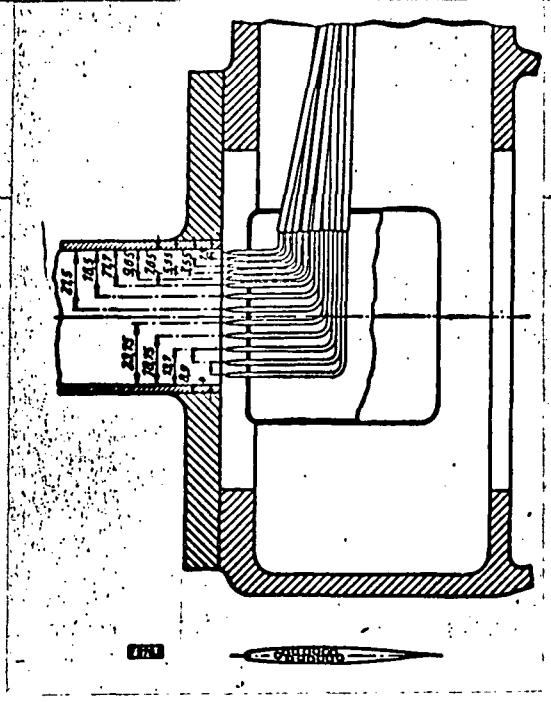

Figure 3. Stagnation tube installation for producing the velocity profile over the final tube cross section.

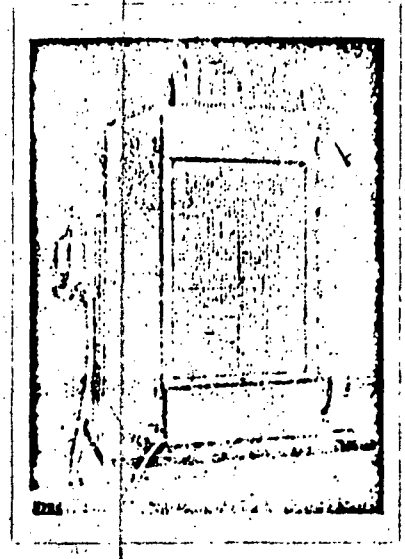

Figure 4. Multiple manometer

be photographed. A stroboscopic valve was installed so that there would be no pressure fluctuations in the pressure indicating instruments. It carries this name because it connects each measurement point with the corresponding manometer in the multiple manometer only when the same pulsation state prevails.

The stroboscopic valve is shown in Figure 5. A distributor a is mounted on a support b so that it can rotate freely. It is driven through a chain wheel c by means of an electric motor. The chain wheel d mounted on the same shaft transfers the rotational motion to the rotational slide so that the slide moves half as fast as the shaft. During one rotation of the shutoff device, two pulsations are carried out. The distributor runs in a carefully designed lining e, which is pressed against the distributor by means of the spring f. The lever g prevents it from rotating with it. Two crowns for pressure connection h can be seen on the lining. Seen from the side, they cover each other exactly. A hole i in the distributor is exactly opposite each crown. These holes are connected with the taps k by means of the longitudinal holes. The two pressure connections l at the lining end at these taps. /172

Pressure differences can be measured with this stroboscopic valve. For example, we can measure the stagnation pressure as the difference between the total pressure at the stagnation probe and the effective static pressure pressure at the stagnation pipe box e (see Figure 1). In order to do this, one of the stagnation probes is screwed into one of the pressure connections l and the pressure tap of the stagnation pipe box is connected with the other connection l. The total pressure will then pulsate in one of the taps k and the box pressure will pulsate at the other one. Since the distributor makes one revolution during a pulsation, the connection h of each crown is subjected to the same pulsation state, that is the same pressure, by means

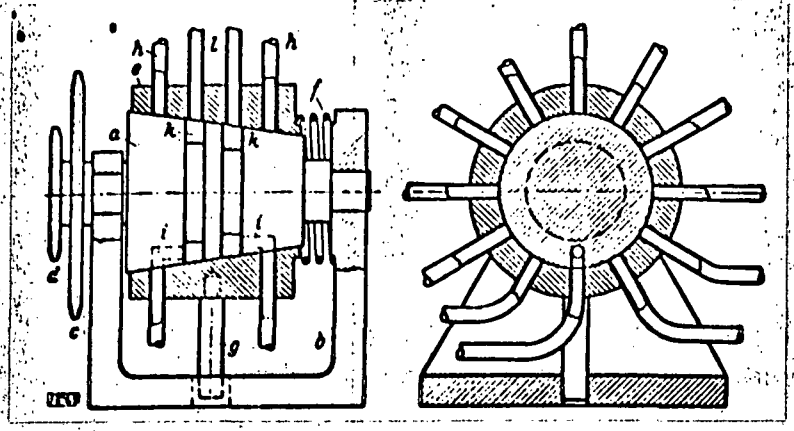

Figure 5. Stroboscopic valve

of the holes i. Each hole h then receives the corresponding pressure over the short time during which the hole i runs by it. This then brings about a long adjustment time of the pressure indication instruments. On the other hand, we are certain that pressures will be measured at certain approximate times, and it is not average values over large time intervals which are being measured. Two connections h which have the same position as seen from the side are connected by means of a U pipe with branches which are curved downward. The U pipes are adjacent to each other in the multiple manometer. In this way simultaneously occurring stagnation pressures occur next to each other on the manometer. The pressure course is displayed at twelve times during a pulsation corresponding to the twelve connections on each crown. It was possible to measure twelve intermediate points after performing a phase displacement of the stroboscopic valve. This meant that 24 measurement points were obtained per pulsation.

The stroboscopic valve requires a longer adjustment time for the manometers. Because of the inertia of the water columns

in the connection pipes, it increases with the pulsation frequency. In spite of the large stagnation pipes, it was only possible to measure up to 24 pulsations per minute. The adjustment time amounted to several hours in this case.

In order to make sure that the average mass flow per pulsation does not change during an experimental test series, the expansion tank a (see Figure 1) was also connected with a special multiple manometer pipe. The expansion tank pressure was maintained constant at 416 mm Hg column, which was done by controlling the water pump.

2. LIMITING CASE OF INFINITELY SLOW PULSATIONS

In order to obtain the limiting case of infinitely slow pulsations, the steady flux was measured for various rotational angles α of the cylinders c in the rotational slide (see Figure 2). It was only possible to test the accuracy of the stagnation pressure indication, which is questionable because of the large stagnation pipe diameter. Also, we were only able to determine the resistance of the experimental pipe and the flux through the capping device as a function of the rotational angle x. During these measurements, of course the stroboscopic valve was dismounted and the pressure measurement points were directly connected with the multiple manometer. We will assume that the laws of turbulent flows in pipes [4] are known, as well as the method of carrying out experiments and their evaluation [3] for steady flow conditions. We will therefore restrict ourselves to a description of the experimental results. Figure 6 shows the pipe resistance coefficient

$$\lambda = -\frac{2d}{\rho \bar{w}^2}\frac{dp}{dx} \qquad (1)$$

determined from the measured pressure difference $-\frac{dp}{dx}$ and the average flow velocity $\bar{u}$ obtained from container measurements (d pipe diameter, ϱ density) as a function of the Reynolds number Re = u d/ν (ν kinematic viscosity). The measurement points labeled 1, 2, 3 were measured at the beginning of the experiment using pulsating flow. The measurement points 4, 5, 6, 7 refer to measurements carried out shortly before termination of the experiment. The Blasius line [5] is also shown for comparison purposes.

The measured velocity profiles are plotted in Figure 7 in the form $u/v_* = f(\lg y v_*/\nu)$ (u, velocity at a distance y from the pipe wall, $v_* = \sqrt{\tau_0/\varrho}$ - shear stress velocity, τ_0, wall shear stress). This /173 was done because in this representation, the profiles are almost straight lines, which run parallel with the profile lines of a hydraulically smooth pipe, which is also shown in the figure. The experimental points lie above the latter line, which would mean that the experimental pipe is even smoother than the hydraulically smooth pipe. However this is due to a systematic measurement error, which is caused by the large stagnation pipe outlets. These caused a restriction of the pipe outlet cross section and therefore bring about higher velocities. In order to reduce this effect, the stagnation pipes are installed at a distance of 2.3 mm from the final cross section as mentioned above, which is relatively far away.

The measurement error can be determined by calculating the actual velocity profiles which occur in the pipe from the pressure decrease. First of all the equivalent sand roughness k_s of the experimental pipe must be determined. The equivalent sand roughness k_s is the sand grain size of a pipe which has been artificially roughened with sand according to Nikuradse [6], which has the same pipe resistance coefficient λ for the same pipe diameter in the range of the quadratic resistance law as

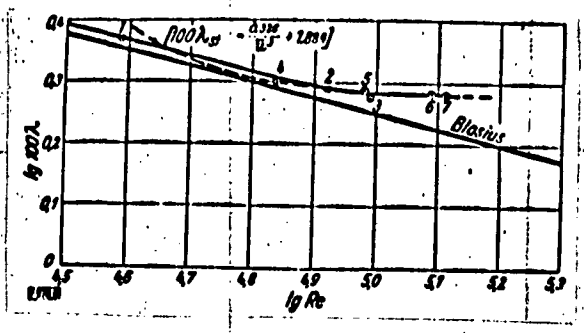

Figure 6. Resistance of the experimental pipe for steady flow.

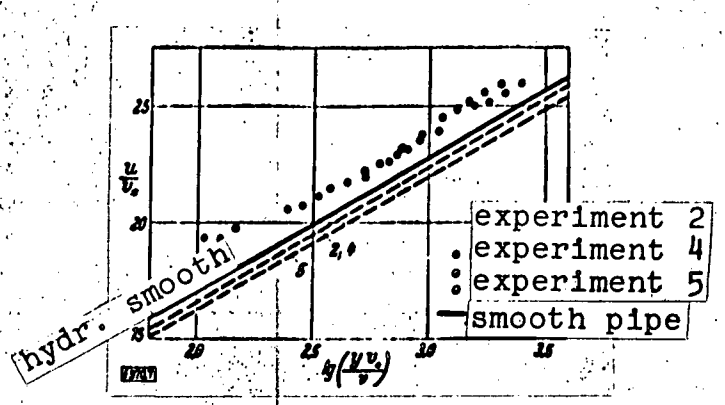

Figure 7. Velocity profiles for steady flow

does our experimental pipe within the range of the quadratic resistance law. Since because of the small roughness of the experimental pipe, the square range only begins at Reynolds numbers $\bar{u}\, d/\nu$ which can no longer be simulated in experiments, we must use the following approximation method:

In Figure 6, resistance curves are drawn through the experimental points 2, 4, 5 for which the velocity profiles are shown in Figure 7. Except for an additive constant, they represent the same function of Reynolds number as for the hydraulically smooth pipe.

For the smooth pipe we have [5]

$$\frac{1}{\sqrt{\lambda}} = 2{,}0 \lg (\mathrm{Re}\sqrt{\lambda}) - 0{,}8 \qquad (2)$$

We will introduce the shear stress velocity $v_* = \sqrt{\tau_0/\varrho}$. From the equilibrium conditions of a cylinder filled with water having the radius $R_0 = d/2$ we obtain

$$-\pi R_0^2 \frac{dp}{dx} = 2\pi R_0 \tau_0$$

and from this we find

$$-\frac{dp}{dx} = \frac{2\tau_0}{R_0} = \frac{2\varrho v_*^2}{R_0}.$$

By introducing the resistance coefficient λ according to equation (1), we find

$$v_*^2 = \frac{\lambda}{8} \bar{u}^2 \qquad (3)$$

so that from equation (2) we obtain the following because $\mathrm{Re} = u\, d/\nu$

$$\frac{1}{\sqrt{\lambda}} = 2{,}0 \lg \frac{v_* R_0}{\nu} + 0{,}7 \qquad (4)$$

We thus obtain a function of the resistance coefficient of the smooth pipe, which we will use as a point of departure. For the experimental pipe we will now write

$$\frac{1}{\sqrt{\lambda}} = 2{,}0 \lg \frac{v_* R_0}{\nu} + K \qquad (5)$$

and we will determine the constant K in such a way that this function will pass through one of the mentioned experimental

points shown in Figure 6. Table 1 shows the calculation. The numbering of the experiments corresponds to that given in Figures 6 and 7.

We will now use the universal roughness function of a rolled industrial pipe, which was determined elsewhere [7] from pipe resistance measurements of Bauer [8]. It will be assumed that this function shown in Figure 8 is also valid for our experimental pipe; then we found that this approximation can be used for a moderately rough surface like the one our experimental pipe had. In the diagram shown in Figure 8, equation (5) is a family of parallel lines, because it can be transformed into the equation /174

$$\frac{1}{\sqrt{\lambda}} - 2{,}0 \lg \frac{R_0}{k_s} = 2{,}0 \lg \frac{v_0 k_s}{\nu} + K.$$

By multiplying by 2.83 and adding 3.75 we find

$$B_r = \frac{2{,}0}{\sqrt{\lambda}} - 5{,}8 \lg \frac{R_0}{k_s} + 3{,}8 = 5{,}8 \lg \frac{v_0 k_s}{\nu} + 2{,}0\,K + 3{,}8,$$

This quantity is plotted in Figure 8 as an ordinate value. If we use K = 0.7, the value which corresponds to the smooth pipe according to equation (4), we obtain the solid line shown in Figure 8. Parallel lines are obtained with the other K values given in Table 1. According to our assumption, only the intersection points with the assumed roughness function will have any physical meaning. The intersection points therefore correspond to the experimental points in Figure 6. In this way we have transferred the experimental points of Figure 6 to the general roughness function shown in Figure 8. The values of $v_* k_s/\nu$ and B_r which correspond to the intersection points are shown in Table 1. Since v_*, ν is known from our experiments, we can calculate k_s from them. If the roughness function of Figure 8

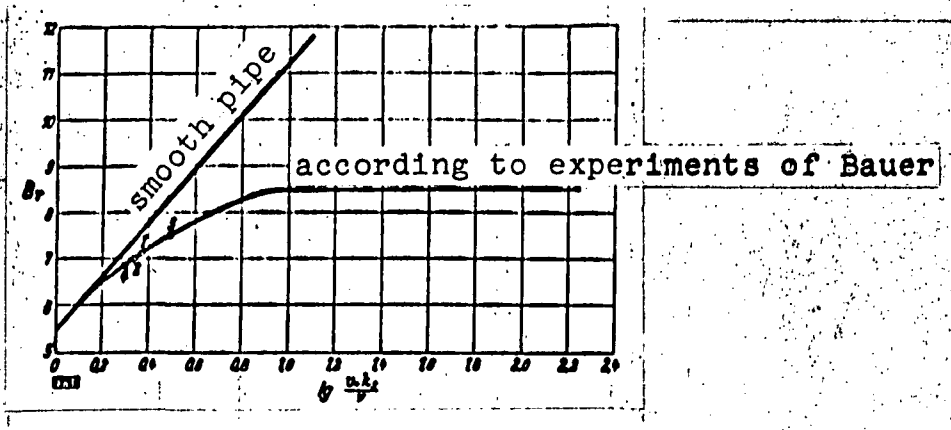

Figure 8. Roughness function for moderately rough surfaces $B_r = 2{,}9\sqrt{\lambda} + 3{,}8 - 5{,}8 \lg r_0/k_s$.

were really valid in our experimental pipe, then only a single k_s value should have been obtained in all our experiments. Table 1 shows that the order of magnitude of the k_s values has not changed during the experiments, which could already have been derived from the position of the experimental points shown in Figure 6.

We will now again consider the velocity profiles. For rough pipes we have the relationship

$$\frac{u}{v_0} = 5{,}8 \lg \frac{y}{k_s} + B_r.$$

In addition we can also derive a relationship having the form

$$\frac{u}{v_0} = 5{,}8 \lg \frac{y v_0}{\nu} + B_g,$$

for the rough pipe according to which the profiles shown in Figure 7 are plotted. B_g is a constant which remains to be determined. B_r has been determined from the roughness function shown in Figure 8. Because these relationships are identical, it follows that

NUMERICAL TABLE 1

STEADY TUBE RESISTANCE VALUES, CALCULATION OF THE VELOCITY PROFILES.*

Experiment Number	$\bar{u}$ cm/s	ν cm²/s	lg 100 λ	lg Re	v_* cm/s	K	lg $\frac{v_* k_s}{\nu}$	$k_s \cdot 10^2$ cm	B_r	B_g
1	89,4	0,01152	0,369	4,59	4,83					
2	191,0	0,01159	0,288	4,92	9,42	0,56	0,34	2,7	7,0	5,0
3	226,6	0,01152	0,274	4,99	10,97					
4	143,6	0,01031	0,301	4,84	7,18	0,59	0,31	2,04	6,85	5,1
5	196,6	0,01031	0,288	4,98	9,65	0,43	0,49	3,28	7,5	4,7
6	254,0	0,01031	0,283	5,09	12,42					
7	269,0	0,01031	0,279	5,11	13,10					

* Commas indicate decimal points.

$$B_g = B_r - 5{,}8 \lg \frac{v_* k_s}{\nu}.$$

The B_g values calculated from this are also shown in Table 1. /175 Now that B_g is known, everything is known in order to plot the velocity profile in our experimental pipe. This is shown as a dashed line in Figure 7. The corresponding experimental points lie above this line. The difference is the excess indication of the stagnation pipe, that is, the systematic measurement error. On the average, the excess indication of average flow velocity u amounts to

7.4%

This error was also obtained by comparing the flow rates determined from container measurements with those obtained by integrating the measured velocity profiles. The integration, which will be discussed later on, resulted in an excess of 7.6%, practically the same amount.

Figure 9 shows the average flow rates, which resulted for various rotational angles a of the cylinder c in the capping unit from container measurements. The differences in the axial displacements L of the cylinder c at which these measurements were carried out correspond to the later experiments

with pulsation. At L=22.4 the cylinder c position is such that the minimum aperture cross section of the capping unit is zero at a certain rotation angle a.

In Figure 9, the flow rate can be decomposed into a constant component u_k and a pulsating component u_p. If we use a bar to indicate average values averaged over the cross section and if we use two bars to indicate subsequent average values over the cross section and the time, then we have

for the instantaneous values: $\bar{u} = \bar{u}_k + \bar{u}_p$

for the average over time: $\bar{\bar{u}} = \bar{u}_k + \bar{\bar{u}}_p$

These values are shown in Table 2 for various displacements L. Subscript B means that $\bar{u}$ was determined from container measurements.

Figure 9 contains a dashed sine curve in order to compare the deviation of the $\bar{u}$ curve from the sinusoidal shape at L=22.4. As far as the deviation of the other curves from the sinusoidal shape is concerned, we would like to remark that the amplitude would be $\bar{u} = \bar{u}_p$ and the maximum value would be $\bar{u}_{max}^* = \bar{u}_k + 2\bar{u}_p$ for the sinusoidal shape. Here the star refers to differentiation from the actual maximum value. $\bar{u}_{max}^*$ and u_{max} are also shown in Table 2.

3. EXPERIMENTS WITH PULSATION*

a) Velocity profiles, reverse flow effects -- The velocity profiles were measured during three experimental test series. The first two test series have the same pulsation duration, which

(*) The kinematic viscosity of the water was $\nu = 0.0105$ cm^2/sec. in this experiment and all other experiments.

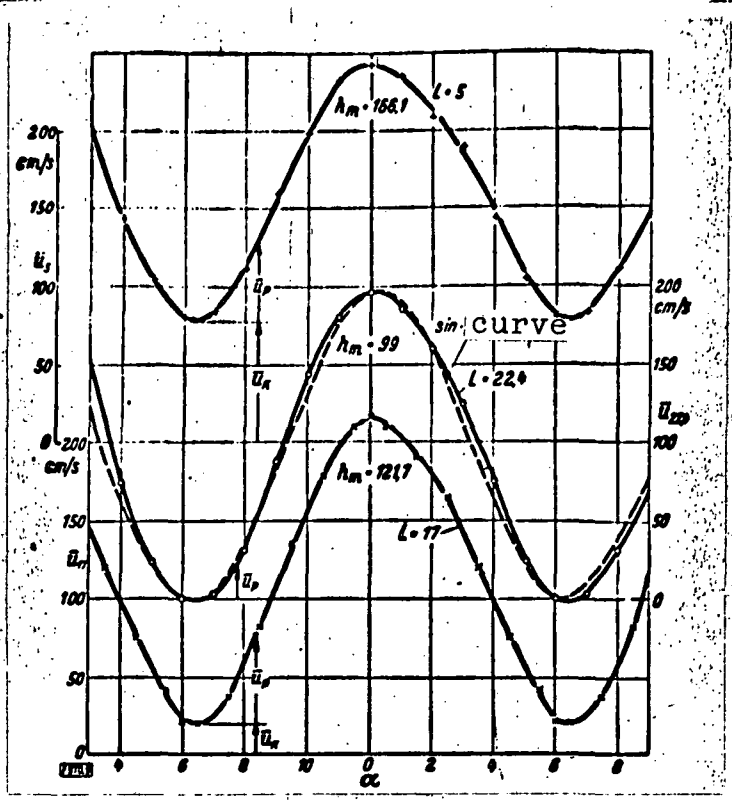

Figure 9. Flow velocity for infinitly slow pulsation, plotted against the rotation angle of the capping unit.

NUMERICAL TABLE 2

AVERAGE LOW VELOCITIES FOR INFINITELY LONG PULSATION DURATION ACCORDING TO CONTAINER MEASUREMENTS. CONSTANT AND PULSATING COMPONENTS.

L	$\bar{u}_B$ cm/s	$\bar{u}_p$ cm/s	$\bar{u}_k$ cm/s	$\bar{u}_{max}$	$\bar{u}_{max}$ *
17	122	102	20	217	224
22,4	101	101	0	193	202
5	166	88	78	242	234

is T=30 sec but differing positions L, that is L=17 and L=22.4. In the third series, the duration of a pulsation was 2.5 seconds and we had L=5. Table 3 shows a summary of the three test series.

/176

Figures 10a through c show examples of the velocity read off the multiple manometer as a function of time. One interesting result is found. Instability begins if there is sufficient retardation. Numerous additional measurements showed that during the retardation period, there is a relatively sudden strong scatter of the measurement points. This phenomenon was especially pronounced in the velocity profiles which are shown for times just before (α=4) and at the beginning of scatter (α=5) and also during the subsequent acceleration period (α=10; 10.5) in the measurement series II shown in Figure 11. Figures 10a and b also shown that negative velocities can occur after the beginning of scatter. However, the true size of these velocities is not indicated because they were measured with stagnation pipes for which the incident flow came from behind.

Figures 12a to c give additional information in the form of a number of successive streamline photographs. During an investigation of a completely different nature, we determined the retarded flow of water with a free surface in a horizontal rectangular channel. The flow has been made visible with aluminum powder which was dropped on the water. The water motion runs from below to above in the photographs. Water is furnished to the channel from a large reservoir. The retardation is first produced only by a level reduction in the container. Later on this comes about by closing the slide at the end of the channel. Figure 12a shows the separation at the curve right channel wall, which is well known from the steady state experiment. The lowest figure shows the retardation in the development of a vortex along the right channel wall, which is the primary effect.

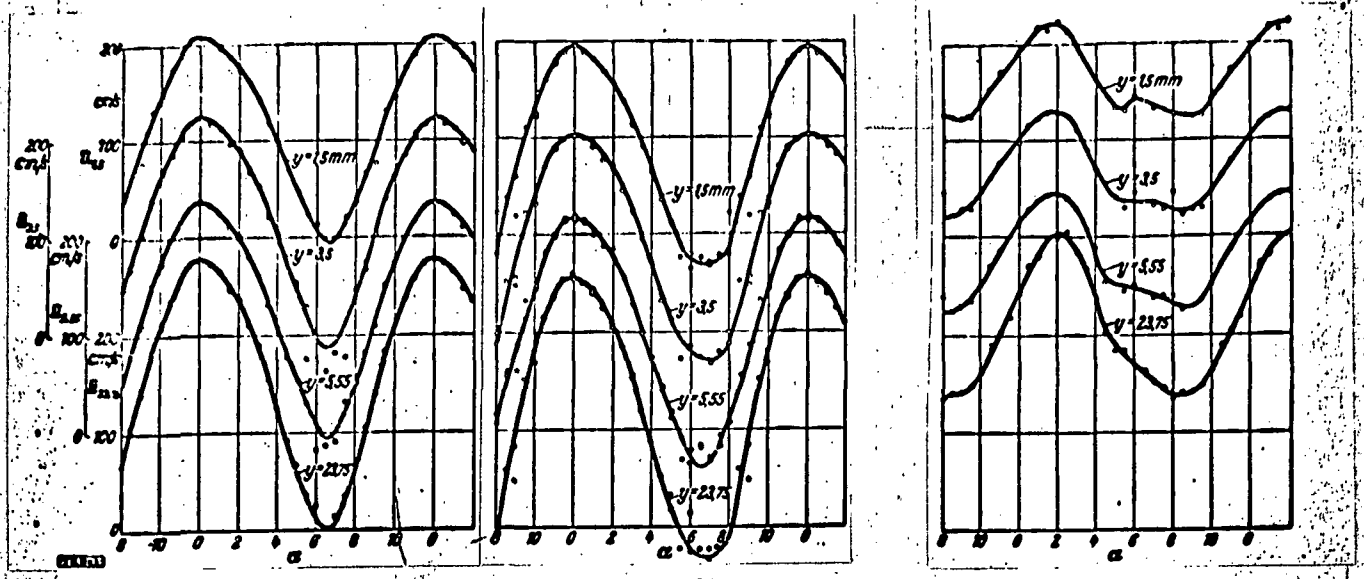

Figure 10a. Measurement series I

Figure 10b. Measurement series II

Figure c. Measurement series III

Figures 10a to c. Velocity course for four different wall separations.

NUMERICAL TABLE 3

COMPARISON OF THE AVERAGE FLOW RATES IN THE CASE OF PULSATIONS DETERMINED BY CONTAINER MEASUREMENTS ($\bar{u}_R$) AND BY INTEGRATING THE VELOCITY PROFILES ($\bar{u}_I$) ; u_p, PULSATING COMPONENT; $\bar{u}_k$, CONSTANT COMPONENT.

Measurement Series	L mm	T s	$\bar{u}_I$ cm/s	$\bar{u}_R$ cm/s	u_p cm/s	$\bar{u}_k$ cm/s
I	17	30	131	121	115	6
II	22,4	30	—	100	101	0
III	8	2,5	180	162	48	114

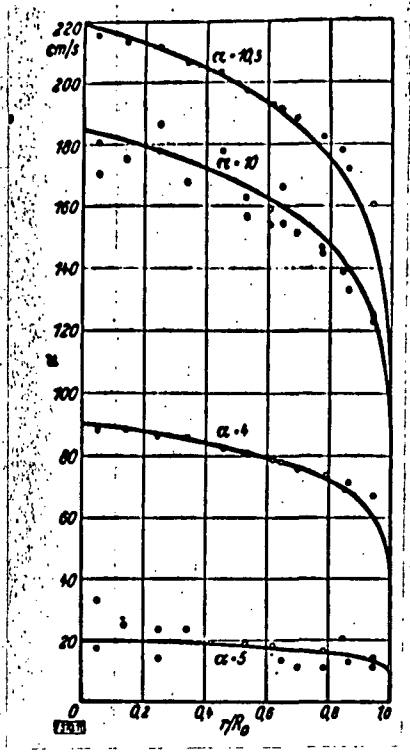

Figure 11. Velocity profiles for certain times α (rotational slide positions) demonstrate the instability because of the scatter in the measured points; comparison with 1/7 parabolas.

Fig. 12a Fig. 12b Fig. 12c

Figure 12a. Separation at a curved surface, development of a vortex along the right channel wall.

Figure 12b. Additional vortex formation.

Figure 12c. Complete vortex development of the space just before closing the slide.

Figures 12a to c. Retarded channel flow

The lowest figure shows the retardation in the development of a vortex along the right channel wall, which is the primary effect. Figure 12b shows that additional vortices have been produced at the channel walls. In Figure 12c, just before the slide is closed, only a vortex motion is present. For completeness, Figures 13a to c also show a startup flow from rest, which is an ordered motion according to expectations.

These observations show that the instability manifests itself by a pronounced vortex motion. Reverse flows can occur at points with a sufficiently small flow rate. Reverse flows are therefore caused by the same factors as separation in the steady case, that is by a pressure increase. In our case the pressure increase is caused by a time delay. Separation is produced by local retardation. /177

Table 3 in connection with Figures 10a through c shows the influence of flow velocity on the initiation of reverse flow. In the case of experiment series I, not as much reverse flow occurs as in experiment series II. In the case of I, the constant component $\bar{u}_k$ of the flow velocity is larger than for II. We will show later on how this influence can be characterized by a parameter if a similarity analysis is performed.

One of the effects of the instability on the pipe flow is the fact that it brings about a considerable increase in the turbulence; this decreases only gradually during the acceleration period, which is indicated by the gradual decrease in the scatter of the experimental points.

b) Testing of the stagnation pressure measurements in pulsating flow.-- The stagnation pressure indications for pulsating flow can also be tested by determining the average mass flow

Fig. 13a Fig. 13b Fig. 13c

Figure 13a. Slide still closed, the water is at rest.

Figure 13b. When the slide is open, the water moves without vortex formation.

Figure 13c. Accelerated motion at a later time.

Figures 13a to c. Accelerated channel flow.

NUMERICAL TABLE 4

DETERMINATION OF THE EXPONENT n OF THE INTERPOLATION PARABOLA.

α . . .	1	2	3	4	10	11	12
n . . .	7,42	7,02	6,81	7,00	6,53	7,17	7,40

by integrating the measured velocity profiles over the cross section and time. These are then compared with the container measurements. The integration is inaccurate because due to the large stagnation pipe diameter. The stagnation pipe closest to the wall (see Figure 3) measures values which are too high and therefore this stagnation pipe had to be eliminated in the evaluation. The next stagnation pipe was at a distance of 3.55 mm from the wall. In order to obtain an interpolation over this distance which would be as accurate as possible, we introduced parabolas in measurement series II of the form

$$\frac{u}{U} = \left(\frac{y}{R_0}\right)^n$$

(u velocity at the wall distance y) for the measured velocity profiles. U and n were selected such that the parabolas intersected the measurement point close to the wall, that is at the wall distance y=3.55 mm and at a point in the vicinity of the pipe center, that is, at a wall distance of y=23.75 mm. The values of n which resulted for the various rotation angles α of the capping unit are shown in Table 4. The average value is

n=7

On the average, and to a good degree of approximation, the 1/7 velocity distribution law results. This is why we performed the interpolation above the wall distance 3.55 mm using 1/7 parabolas. Figure 14 shows the flow velocities averaged over the cross section as obtained using this interpolation by integrating the velocity profiles. The corresponding flow velocities are /178 compared with the container measurements in Table 3. From this we find a reading of the stagnation pipes which is consistently too large, in agreement with the excess reading for the steady case mentioned at the beginning. The stagnation pipe measurements are too large by the following factors according to velocity

for measurement series I 8%
for measurement series III . . . 11%.

These percentages were used to correct the velocities during the evaluation.

Measurement series II was corrected in the same way as measurement series I. Since these are average correction values, the instantaneous values of the velocities will remain inaccurate nevertheless, especially for measurement series which showed

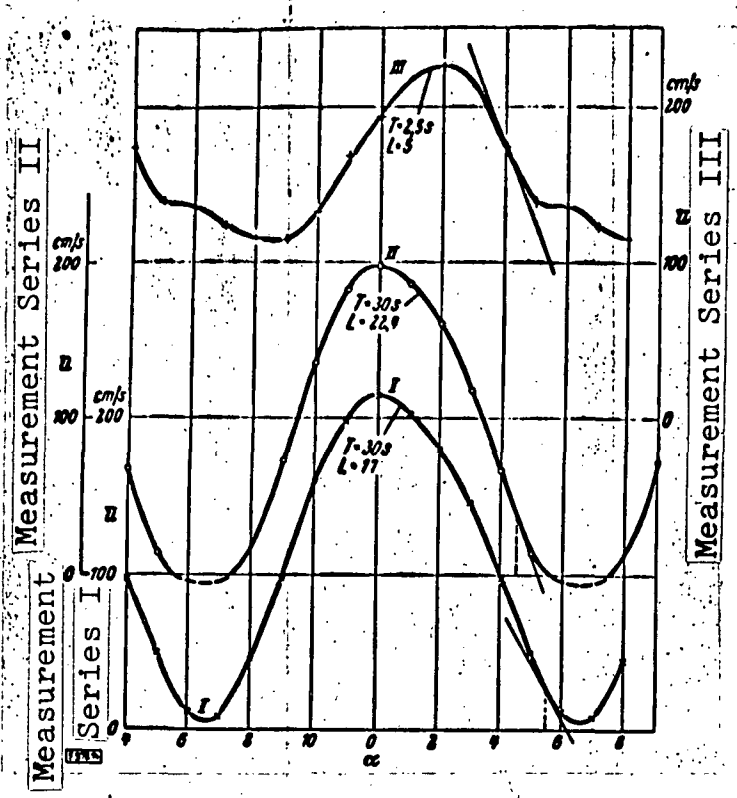

Figure 14. Time behavior of the average flow rate $\bar{u}$, measurement series I, II, III.

that there was reverse flow which could not be measured. Therefore the correction was not evaluated for the measurement series II, which had the greatest amount of reverse flow. This inaccuracy later on has an effect on the determination of the pipe resistance, because the third power of the velocities $\bar{u}$ is required for this.

c) Influence of inertia on the pulsation history -- We pointed out that with the experimental arrangement introduced, the pulsation is not positively controlled, because the inertia of the water column enclosed in the pipe can influence the pulsation process. We will now calculate the influence of this effect, because it was not possible to measure the average flow velocity as a function of time for all the frequencies of

interest. The momentum theorem applied over the entire pipe distance, which had a length of x=9.31 m, results in

$$\varrho \frac{d\bar{u}}{dt} x = p_1 - p_2 - \Delta p_r \qquad (6)$$

where p_1 is the pressure at the inlet cross section, p_2 the pressure at the outlet cross section and Δp_r is the pressure difference required to overcome the pipe friction. Since the experimental section was connected to an expansion tank, we have p_1=const. , and we had p_1=5250 mm water column.

The pressure p_2 is determined according to the outflow number μ of the rotational slide, which is determined by the formula

$$\bar{u}_H = \mu \sqrt{\frac{2}{\varrho} p_2}$$

$\bar{u}_H$ is the outflow velocity at the outlet cross section F_H of the rotational slide. Since $\bar{u}F_R = \bar{u}_H F_H$ (F_R pipe cross section), we can introduce an outflow coefficient $\mu' = \mu F_H / F_R$ which refers to $\bar{u}$

$$\bar{u} = \mu' \sqrt{\frac{2}{\varrho} p_2} \qquad (7)$$

Here we are only interested in $\bar{u}$ and not $\bar{u}_H$. μ' depends on the angular position of the capping valve. For our frequency range it apparently only depends slightly on the pulsation frequencies and on the reverse flow effect. The latter two influences will not be considered, but this will be tested by carrying out an experiment to investigate this error.

If there is no frequency dependence, we can determine μ' in the steady case at various angular positions α of the capping

valve. In other words we can determine it for an infinitely long pulsation duration. In equation (6) we then have $du/dt=0$. In addition the friction pressure drop can be ignored: $\Delta p_r=0$. Then we have $p_2=p_1$ according to equation (6) and we obtain the following by introducing the numerical values given above in equation (7),

$$\mu' = \frac{\bar{u}_0}{10{,}18} \qquad (8)$$

where $\bar{u}_0$ is in meters/sec. Subscript 0 means that this is the flow velocity for the steady case. /179

In order to see whether this relationship can be used for pulsations, we measured the pressure p_2 at the outlet cross section as a function of the angular position α. This was done for measurement series I and II and is shown in Figure 15. The result is shown in Figure 16 in which the measurement points deviate from the straight line corresponding to equation (8). We may therefore say that the outflow coefficient μ' given by equation (8) also determines the pressure p_2 according to equation (7) in the case of pulsation.

In order to formulate the unsteady case, momentum equation (6) is introduced in equation (7). If Δp_r is again ignored, we obtain

$$x\frac{d\bar{u}}{dt} = \frac{p_1}{\varrho} - \frac{\bar{u}^2}{2\mu'^2} \qquad (9)$$

which determines $\bar{u}$. It is solved while restricting ourselves to small $d\bar{u}/dt$ values by applying stepwise approximations beginning with the limiting case of infinitely long pulsation duration ($d\bar{u}/dt=0$). We also approximate the pulsation in Figure

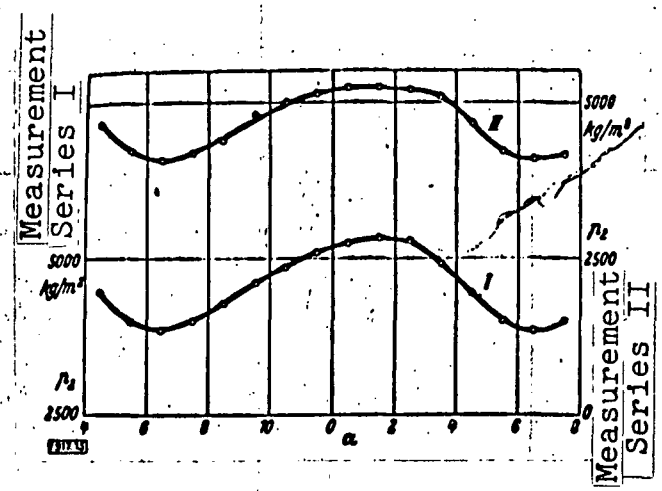

Figure 15. Pressure at the outlet cross section as a function of time, measurement series I and II.

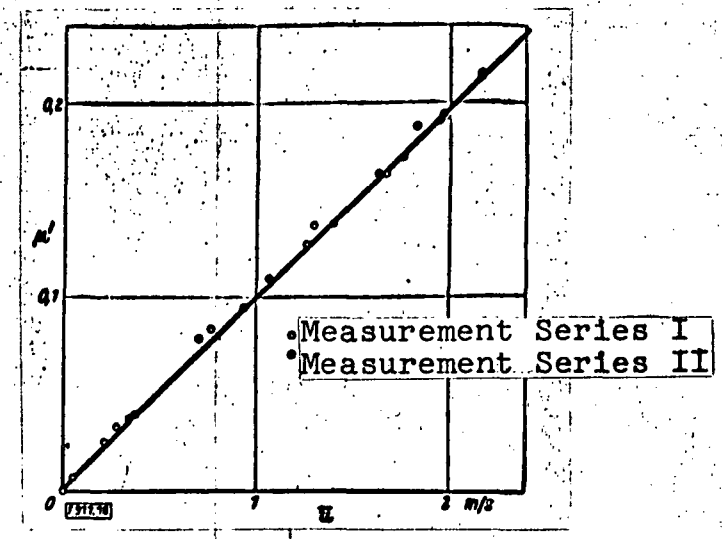

Figure 16. Outlet number μ' of the rotational slide as a function of velocity.

9 by a sinusoidal course as follows:

measurement series I $\bar{u}_0 = 1{,}180 + 0{,}085 \sin \frac{2\pi}{T} t$ in m/s

measurement series II $\bar{u}_0 = 0{,}980 + 0{,}985 \sin \frac{2\pi}{T} t$ in m/s

measurement series III $\bar{u}_0 = 1{,}645 + 0{,}805 \sin \frac{2\pi}{T} t$ in m/s,

where the subscript 0 again expresses the fact that this is the zero approximation ($d\bar{u}_0/dt$ ignored). These expressions now completely determine μ'. The first approximation is obtained from equation (9)

$$x \frac{d\bar{u}_0}{dt} = \frac{p_1}{\varrho} - \frac{\bar{u}_1^2}{2\mu'^2},$$

and from this we find

$$u_1 = \mu' \sqrt{2} \sqrt{\frac{p_1}{\varrho} - x \frac{d\bar{u}_0}{dt}}$$

The n-th approximation is as follows, if we develop the root in a series, since $d\bar{u}_0/dt \ll p_1/\varrho$

$$\bar{u}_n = \mu' \sqrt{2} \sqrt{\frac{p_1}{\varrho}} \left(1 - \frac{x}{2} \frac{\varrho}{p_1} \frac{d\bar{u}_{n-1}}{dt} \ldots\right).$$

We will restrict ourselves to the second approximation and we obtain the corrections shown in Figure 17a through c at the various frequencies to be applied to the course of $\bar{u}$ due to inertia. The correction for L-5; T-4 sec is not given.

d) Pressure decrease -- Figures 18a through c show the measured pressure drops as a function of the angular position α of the capping unit. Each curve shows the corresponding time duration T of one pulsation. We could not remove the large

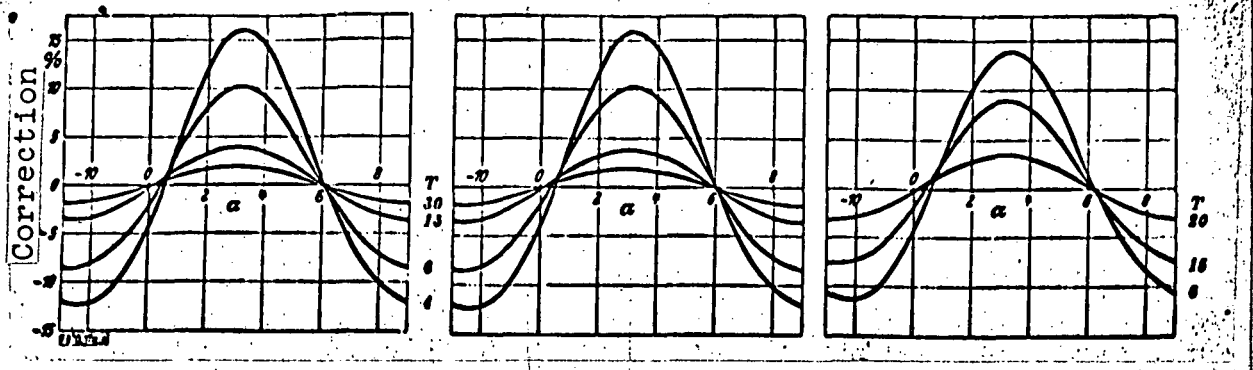

Figure 17a. L=17 Figure 17b. L=22.4 +Figure 17c. L=5

Figure 17a to c. Inertia corrections for the force of $\bar{u}$ made to the various frequencies T in the experiment.

scatter in the experimental points, especially at higher frequencies. These are caused by the reverse flow effect.

/180

The pressure decrease must overcome the pipe resistance and must accelerate the water column contained in the pipe. The friction pressure decrease pulsates with the flux, because it is a function of the velocity. The pressure decrease required for acceleration pulsates with the acceleration. In the case of sinusoidal pulsation, it has a 90° phase displacement with respect to the flux. For slower pulsations, the friction pressure decrease dominates. For fast pulsations, the acceleration pressure decrease dominates. Therefore we can expect a displacement in the maxima of the pressure decrease curves as the pulsation frequency is increased. This was indeed found in the measurement results. In addition, at higher frequencies, the retardation produces a considerable pressure increase over a short time.

/181

In addition, for L=17 and l=22.4 and T=30 sec we showed the course of the pressure decrease which is required to only accelerate the water column by means of a dashed curve. This

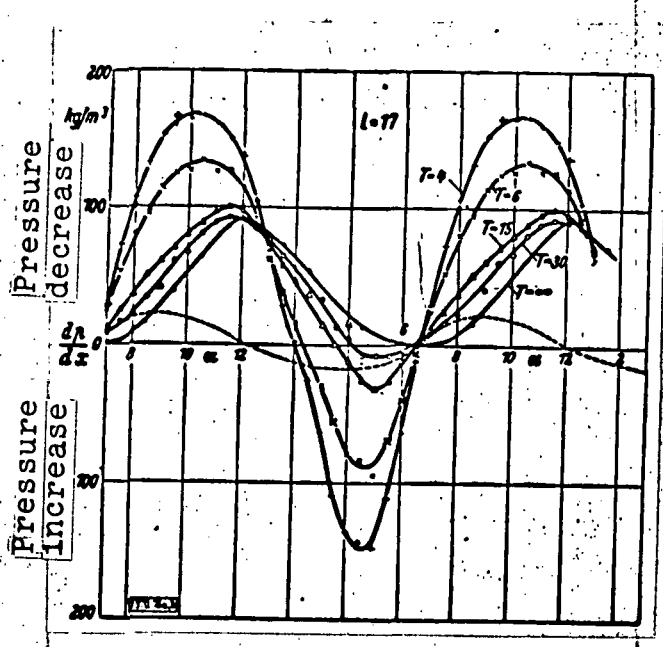

Figure 18a. L=17

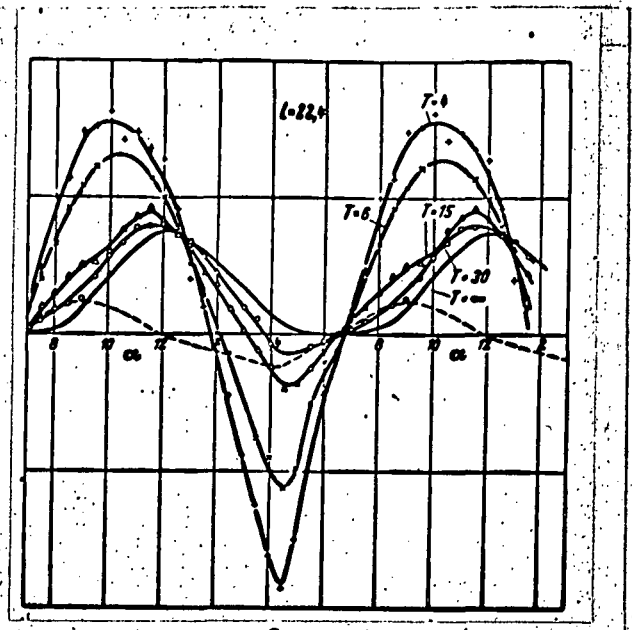

Figure 18b. L=22.4

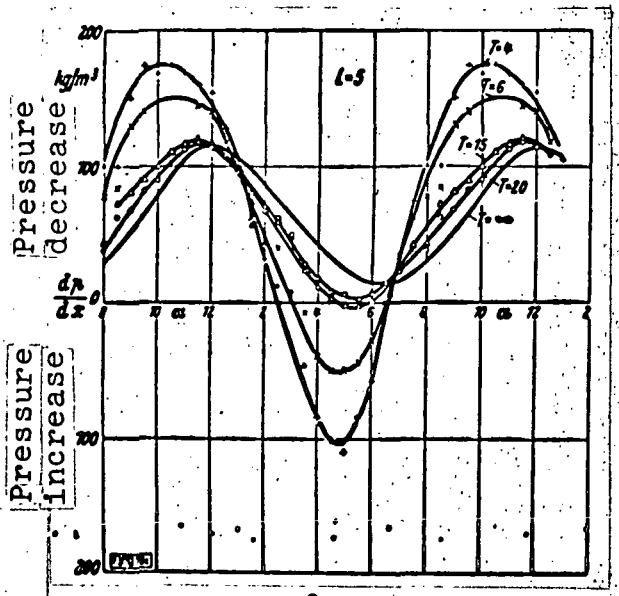

Figure 18c. L=5

Figure 18a to c. Course of the pressure decrease for various pulsation frequencies.

is obtained after differentiation of the curve for $\bar{u}$ shown in Figure 14 which is obtained by means of the momentum theorem taken over the pipe cross section and for a frictionless fluid

$$\frac{d\bar{u}}{dt} = -\frac{1}{\varrho}\frac{dp}{dx}$$

The pressure decrease required to overcome the friction dominates for this long pulsation time.

4. CLOSER INVESTIGATION OF THE FRICTION RESISTANCE DURING A PULSATION.

After the variation in the pressure decrease and flow velocity with time are known, the average resistance power W per unit of length and cross section of the pipe over one pulsation period can be calculated. It is given by

$$W = -\frac{1}{T}\int_0^T \frac{dp}{dx}\,\bar{u}\,dt \qquad (10)$$

Figure 19 shows the course of $\left[\frac{2d}{\varrho}\frac{dp}{dx}\bar{u}\right]$ for the measurement series I plotted as a function of the angular position α of the capping unit. It was obtained from Figures 14 and 18a. With a graphic integration we found

$$W = 70{,}5\ \mathrm{kg/m^2\,s.}$$

This power can be compared with the resistance power W' which is obtained by using the steady state friction law of the experimental pipe and the $\bar{u}$ variation for pulsations. Using the definition equation (1) we find

$$-\frac{dp}{dx}\bar{u} = \frac{\varrho}{2d}\lambda\,\bar{u}^3$$

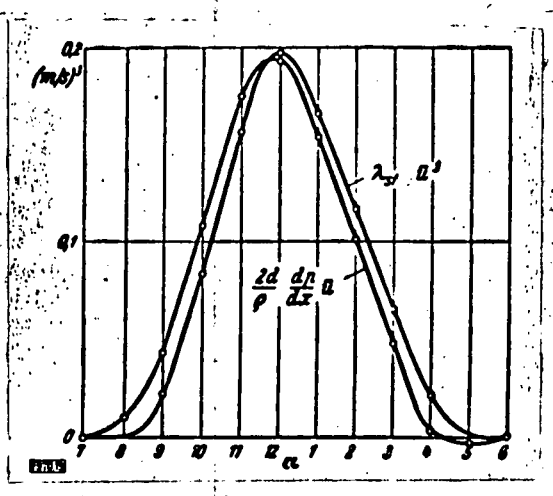

Figure 19. Determination of the friction resistance, measurement series I.

and therefore because of equation (10)

$$W' = \frac{1}{T}\frac{\varrho}{2d}\int_0^T \lambda\, \bar{u}^3\, dt \qquad (11)$$

The steady state friction loss can be represented in the following way as a function of $\bar{u}$ in m/s for lg Re > 4.6 and $\bar{\nu}$=0.0105 cm/s^2

$$100\,\lambda_{st} = \frac{0{,}326}{\bar{u}^3} + 1{,}884,$$

It is shown in Figure 6 by means of dashed lines. For smaller Re numbers, the product $\lambda_{st}\,\bar{u}^3$ becomes vanishingly small, so that it is not necessary to know the exact resistance law. The course of $\lambda_{st}\,\bar{u}^3$ is shown in Figure 19 and from this we find

$$W' = 71{,}4\ \mathrm{kg/m^2s},$$

which is essentially the same value as W. Therefore in this experiment the steady state friction loss is obtained on the average. The changes which are produced by acceleration and retardation approximately cancel each other. Whether this is true for other pulsation amplitudes and frequencies can be decided by means of the characteristic number Γ to be defined later on. In this experiment we found $\Gamma=0.019$. For $0 \leqq \Gamma \leqq 0{,}019$ the above mentioned statement holds, because in this range the acceleration and retardation are even smaller than was the case in our experiment.

It is not possible to make a comparison with the steady state type friction law for the other pressure decrease measurements, because the reverse flow effect brings about an inaccuracy in the third power of the flow velocity $\bar{u}$, so that it is not possible to accurately determine the small deviations from the steady state friction law. Therefore we only compared the pipe friction values for pulsation with each other and with the pipe friction characteristic number

$$\lambda_p = \frac{d}{\frac{\varrho}{2}\bar{u}^3} \cdot \frac{\int_0^T \frac{dp}{dx}\bar{u}\,dt}{T} \qquad (12)$$

λ_p is a measure of the resistance power, because the second factor represents the average value of the pressure decrease which brings about the same power as the actual pressure decrease during a pulsation. In this evaluation, only the third power of $\bar{u}$ is required, which is obtained from the reliable container measurements. The course of $\bar{u}$ was approximately obtained for the various frequencies using the inertia corrections given in Figure 17 using the $\bar{u}$ curve at $T=\infty$ (Figure 9). The Table 5 gives the values of λ_p obtained. It is seen that within

the framework of this approximation, there is no increase in the pipe friction as the Γ parameter is increased up to $\approx 0{,}2$. In addition, Table 1 also gives λ_{st} which is a number calculated from equation (1) using $\bar{u}$.

The $\Delta\bar{u}$ values in Table 5 were also determined with this correction, unless they were directly measured. At L=5 we note a large difference between the calculated $\Delta\bar{u}$ number at T=4 sec and the measured value at T=2.5 sec. It is not so much a consequence of the difference in frequency, but due to the fact that the reverse flow effect and the frequency dependence of μ'. At the higher frequencies, this shows the deviation in our determination of $\bar{u}$ from reality. At T=30 sec we found satisfactory agreement between the calculation and the experiment.

In addition, we can determine the shear stress τ from the following momentum equation applied to a concentric water cylinder having the radius r

$$2\pi\int_0^r r\frac{du}{dt}dr = -r^2\pi\frac{1}{\varrho}\frac{dp}{dx} - 2r\pi\frac{\tau}{\varrho} \qquad (13)$$

However, we encounter the same difficulty as in a nozzle or diffusor experiment. The quantity τ is obtained as the small difference between two numbers. It is therefore very inaccurate.

Figure 20 first shows the distribution of the acceleration and retardation as a function of r^2 at a specific time. It is obtained by differentiating the time history of the velocity. Because of the inaccuracy always associated with graphical differentiation, the experimental points are scattered. However they do lie in the vicinity of an average line. We again use the 1/7 velocity distribution law for interpolation near the

NUMERICAL TABLE 5

PIPE RESISTANCE COEFFICIENTS λ_p FOR PULSATION

	L = 17 mm					L = 22,4 mm					L = 5 mm				
T [s] . .	∞	30	15	6	4	∞	30	15	6	4	∞	15	6	4	2,5
$\bar{u}_B$ [cm/s]	122	121	123	120	119	101	101	101	99	98	166	163	162	161	162
$\bar{u}_k$ [cm/s]	19	6	—	—	—	0	0	0	0	0	78	—	—	—	114
$\bar{u}_p$ [cm/s]	103	115	—	—	—	101	101	101	101	101	88	—	—	—	48
$\Delta\bar{u}$ [cm/s]	99	104	98	98	98	98	99	98	98	98	86	82	82	82	56
$100\,\lambda_p$.	3,7	3,9	4,0	3,9	3,9	4,9	5,2	5,2	5,1	5,1	2,6	2,7	2,7	2,6	—
$100\,\lambda_{stat}$	2,12	2,12	2,12	2,12	2,12	2,24	2,24	2,24	2,24	2,24	1,96	1,96	1,96	1,96	1,96
$Re\cdot10^{-4}$	5,8	5,8	5,8	5,7	5,7	4,8	4,8	4,8	4,7	4,7	7,9	7,8	7,7	7,7	7,7
$\Omega\cdot10^2$.	0	1,2	2,2	5,7	8,7	0	1,6	3,2	8,3	12,7	0	1,0	2,6	4,0	4,3
$\Gamma\cdot10^2$.	0	1,9	3,4	8,9	13,4	0	2,4	4,7	12,3	18,8	0	1,7	4,3	6,7	7,2

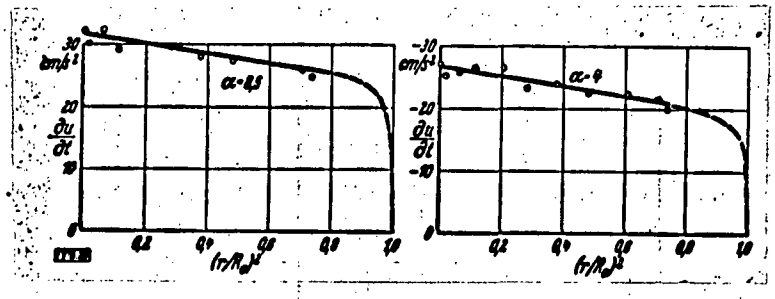

Figure 20. Course of the acceleration (α=8.5) and retardation (α=4), measurement series I.

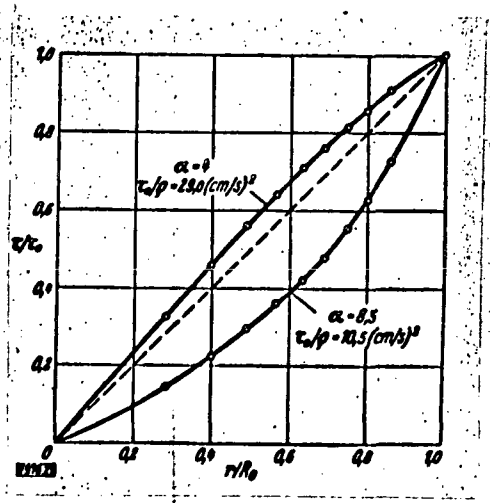

Figure 21. Shear stress distribution over the pipe radius for acceleration (α=8.5) and retardation (α=4), measurement series I.

wall. We find the shear stress profiles shown in Figure 21. We can see that in the case of acceleration (α=8.5) they are displaced downward. For retardation (α=4) they are displaced upwards. In order to clarify this phenomenon we have drawn the dashed line through the end points. Similar phenomena were observed in the experiments of Nikuradse [9] in expanded and contracted channels. In these experiments, the shear stress profiles in the diffusor are curved in the same direction as during the retardation period in our experiments. In convergent channels, the curvature is the same as in our profiles during the acceleration period. Consequently spatial and temporal accelerations operate in the same direction(*).

When equation (13) was applied to measurement series I, during which we found almost no reverse flow as mentioned above, we find the wall shear stress as shown in Figure 22 during the pulsations. For comparison purposes, points are shown in this figure which are obtained according to the steady state pipe friction law and the $\bar{u}$ curve shown in Figure 14. We find here that for acceleration, the friction resistance is somewhat smaller and somewhat larger for retardation than for the steady case.

5. COMPARISON WITH EARLIER PIPE RESISTANCE MEASUREMENTS WITH PULSATING FLOW.

There is an investigation by Estel [2] regarding pipe resistance for pulsating flow. A time average of the pressure decrease was measured there using greatly damped pressure indicating devices. From this a pipe resistance coefficient

(*) The shape of the shear stress profiles can be formulated using the delayed effect hypothesis for turbulence for the retarded flow. See for example F. Schultz-Grunow, The Aftereffect of Turbulence in the Spatial and Temporal Retarded Boundary Layer Flow, Proc. 5. Intern. Congr. Appl. Mech., New York 1939, p. 428.

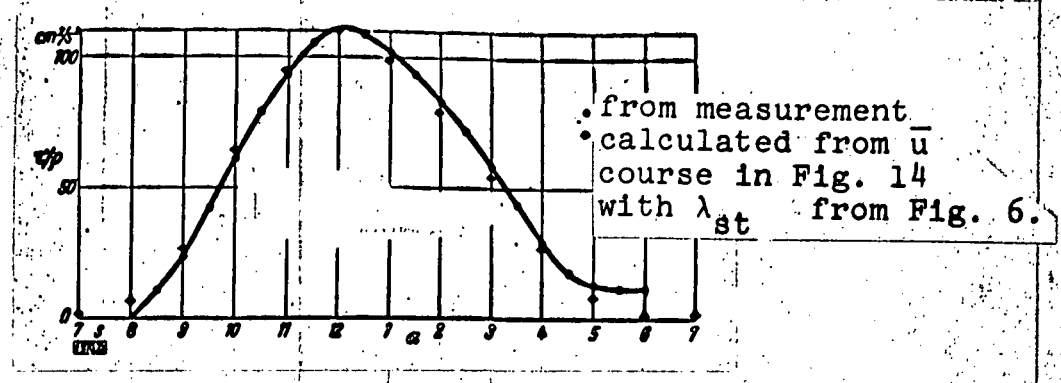

Figure 22. Time course of the wall shear stress, measurement series I.

was determined and it was found that the pulsation increased the pipe resistance. This increase was measured for various experimental conditions.

These results do not show whether a friction law different from the steady state case applies for pulsations, as can be shown by the following discussion. Since strongly damped measurement instruments were used, Estel measured the arithmetic mean

$$\frac{d\bar{p}^*}{dx} = \frac{1}{T}\int_0^T \frac{dp}{dx}\,dt$$

and therefore formed the pipe resistance coefficient

$$\lambda_p^* = \frac{2d\int_0^T \frac{dp}{dx}\,dt}{\varrho\,\bar{u}^2} \qquad (14)$$

We can show that we will always have $\lambda_p^* > \lambda_{st}$, even when the steady friction law applies for pulsations. If we assume that this is the case, then we can express dp/dx by λ_{st}. We then

find

$$\lambda_p^* = 1/T \frac{\int_0^T \lambda_{st} \cdot \bar{u}^2 \, dt}{\bar{u}^2}.$$

In this case, the large velocities make a greater contribution to the integral over $\lambda_{st} \bar{u}^2$ than the small velocities. This is in contrast to the average value $\bar{u}$, for which the large and small velocities make this same contribution. Since λ_{st} changes only slightly in the range of the quadratic friction law and does not change at all with $\bar{u}$, we indeed find /184

$$\lambda_p^* > \lambda_{st}$$

For example, for the smooth pipe and using the Blasius resistance law $\lambda_{st} = \frac{0{,}316}{\sqrt[4]{Re}}$ and $Re = \frac{\bar{u} d}{\nu}$ we find

$$\lambda_p^*/\lambda_{st} = \frac{\int_0^T \bar{u}^{7/4} dt}{T \bar{u}^{7/4}}.$$

Estel called the ratio λ_p^*/λ_{st}, Ψ and determined it experimentally. From the preceding discussion it follows that Ψ is essentially a calculated quantity. It represents a mathematical error caused by taking averages in the wrong way. This is one peculiar feature of the pipe friction law, where the pipe friction is approximately proportional to $\bar{u}^2$. This is why the factor Ψ is approximately the ratio of the quadratic mean to the arithmetic mean. As stated above, it is greater than 1. A very similar error occurs when mass flows are measured in pulsating flows with diaphragms and strongly damped pressure indicating devices. This has been known for a long time [1].

The factor Ψ can be completely avoided if pulsating pipe flows are compared with the quasi-steady flows. We mean by this pipe flow with an infinitely long pulsation duration for which the steady pipe friction law is exactly satisfied. According to our determinations it is also approximately valid for pulsations within certain limits. Therefore the λ_p^* or the λ_p determined for the quasi-steady case can also be applied to pulsations.

6. SIMILARITY DISCUSSION.

Even though the experiments did not show that there was a strong dependence of the pipe resistance on the pulsation frequency, it is nevertheless interesting to determine which parameter describes this dependence. A similarity analysis can provide this information.

We can expect that there is dependence on the Reynolds number $Re = \frac{\bar{u}d}{\nu}$ and on the relative equivalent sand roughness $2\frac{k_s}{d}$, if we consider rough pipes in the discussion. Also there will be a dependence on a parameter which characterizes the type and intensity of the acceleration and retardation. This is obtained by specifying the percentage velocity increase which a liquid particle experiences along a path proportional to the pipe diameter. If this is the same for two cases, then the same acceleration conditions will apparently prevail. The percentage velocity increase in differential form is $\frac{d\bar{u}}{\bar{u}}$ and the corresponding path length proportional to the pipe diameter is $\frac{\bar{u}dt}{d}$, so that the characteristic number is

$$\Omega' = -\frac{d\bar{u}}{dt}\frac{d}{\bar{u}^2}$$

The beginning of reverse flow should be characterized by this

number if we substitute the retardation which occurs just before this time $-d\bar{u}/dt$ and the velocity $\bar{u}$. For simplicity we will assume that only those quantities which occur just before the beginning of reverse flow will be decisive for the reverse flow. If we use the aftereffect hypothesis* we could show which earlier times also have an effect. We will not do this because the essential points have already been stated with this characteristic number.

In order to describe the pipe resistance we will introduce the average value $\bar{u}$ and the amplitude $\Delta\bar{u}$ in the characteristic number because we are only interested in average values over the period. Consequently we will set

$$\Omega = \frac{\Delta\bar{u}}{T}\frac{d}{\bar{u}},$$

which is a number which only involves the average acceleration magnitude and not its dependence on time. Another parameter, which will not be considered here, involves the special type of $\bar{u}$ dependence.

The calculation of Ω' and Ω has been performed and is shown in Tables 5 and 6 for measurement series I, II, III. Figure 14 shows the tangents and ordinates for the inclinations $d\bar{u}/dt$ which were introduced in the calculation. There is a certain degree of arbitrariness in the values of $\bar{u}$ which were used to calculate Ω', because the tangents touch the curves over a long distance and the time at which the reverse flow starts is not exactly specified.

(*) See footnote on page 35.

NUMERICAL TABLE 6

DETERMINATION OF THE CHARACTERISTIC NUMBERS Ω' and Γ' FOR MEASUREMENT SERIES I, II AND III.

L mm	T s	d cm	$\bar{u}$ cm/s	$-d\bar{u}/dt$ cm/s²		$Re^{1/4}$	Γ'
17	30	5	27	15	0,1	11,4	1,14
22,4	30	5	37	20,8	0	13,3	1,10
5	2,5	5	176	245	0,0	20,0	1,16

It is natural to apply the characteristic number Ω' to convergent and divergent channels as well, because similar effects of temporal and spatial accelerations in the shear stress profiles were found. For this purpose we will write Ω' in the form

$$\Omega' = \frac{d\bar{u}}{\bar{u}\, dt}\,\frac{d}{\bar{u}}$$

and consider $d\bar{u}$ as a velocity increase or velocity decrease, respectively, along the path $dx = \bar{u}\, dt$ measured in the flow direction. This results in

$$\Omega' = \frac{d\bar{u}}{dx}\,\frac{d}{\bar{u}}$$

We are thus led to the equivalent characteristic number $\omega = \frac{dU}{dx}\,\frac{d}{2U}$, which Prandtl [10] used as a parameter in the diffusor flow for the relationship between the velocity profile and the pressure increase, assuming that the Reynolds number is constant. U is the maximum velocity over a cross section. If we assume plane diffusor flow, which was investigated by Nikuradse [9], and if we call the diffusor width 2h and if it

increases with x, then we have

$$d = 2h = 2x \operatorname{tg} \beta,$$

where β is 1/2 of the diffusor aperture angle. In addition, if Q is 1/2 of the flow rate per unit of time,

$$\bar{u} = \frac{Q}{x \operatorname{tg} \beta}, \quad \frac{d\bar{u}}{dx} = \frac{Q}{\operatorname{tg} \beta \cdot x^2},$$

and we obtain

$$\Omega' = 2 \operatorname{tg} \beta \approx 2\beta.$$

Ω' is nothing but the diffusor aperture angle. In Nikuradses experiments, the largest angle for which separation was found was β=4°. Thus we find

$$\Omega' = 0{,}14,$$

This is a value which exceeds the corresponding value for pulsating flow (see Table 6). By considering the influence of the Reynolds number, for which Prandtl [10] gave the characteristic number $\Gamma = \omega \mathrm{Re}^{1/4}$ assuming the Blasius resistance law [5], we obtain the following value from Nikuradses experiments for a 4° semi-aperture angle

$$\Gamma = \Omega' \mathrm{Re}^{1/4} = 2{,}2.$$

Assuming that the deviation in the resistance law of our experimental type from the Blasius law can be ignored, which is apparent from Figure 6, we also calculated the characteristic number Γ' in Table 6 for reverse flow in the pipe. We find that

it has a value which is about half as large as for a diffusor. However, the Γ' values for pulsating flow agree completely. The characteristic number Γ' therefore seems to be a criterion for the beginning of reverse flow for time retardation which is quite independent of the type of pulsation.

We have now found that Γ' and therefore also Γ are characteristic numbers which are analogous to a characteristic number derived earlier by Prandtl for nozzles and diffusors. We can therefore say that the resistance coefficients of nozzles and diffusors carrying pulsating flows can be represented by means of resistance diagrams $\lambda = f(\Gamma_p, \Gamma_s)$. Γ_p is the characteristic number formed with the temporal acceleration and correspondingly Γ_s is the characteristic number formed with the spatial acceleration. Therefore we have found a clear ordering of the experimental values. Figures 12 and 13a-c showed the effects of simultaneously acting temporal and spatial retardations and accelerations, respectively. We determined that reverse flows produced by temporal accelerations can be avoided by an additional spatial acceleration. We can expect that λ can be approximately represented by means of a function of $\Gamma_p + K\Gamma_s$ (K constant). Our experiments give information regarding the variation of λ in the range $0 \leq \Gamma_p \leq 0.02$. The present investigations [9] do not give any information regarding the influence of Γ_s. /186

7. PRACTICAL CALCULATION OF THE PIPE RESISTANCE FOR PULSATING FLOW.

In any practical calculation of the pipe resistance, it is important to know that for low characteristic numbers Γ the pulsation does not change the pipe friction appreciably so that we can use the pipe friction law for steady flow as an approximation. However, it is not enough to specify the friction

law. In practice it is important to know what the average resistance power will be which must be expended. The average resistance power was already formulated in equation (10). The resistance coefficient λ_p was established in equation (12), which is a measure of the resistance power, which has to be the case according to its mechanical meaning. The resistance coefficient λ_p^* proposed by Estel [2] is a measure for the average decrease as equation (14) shows. This average value has no practical value and contradicts the mechanical interpretation of the resistance coefficient.

If we now use equation (12) to express the instantaneous value of the pressure decrease by means of the pipe resistance coefficient λ_{st} for the steady case, we obtain the following equation to determine the pipe resistance coefficient λ_p for pulsations:

$$\lambda_p = \frac{\int_0^T \lambda_{st}\ \bar{u}^3\, dt}{\bar{u}^3\, T}.$$

One of the well-know resistance laws can be introduced for λ_{st}; for example, using the Blasius law [5] $\lambda_{st} = \frac{0{,}316}{\sqrt[4]{Re}}$ we find

$$\lambda_p = \bar{\lambda}\, \frac{\int_0^T \bar{u}^{11/4}\, dt}{\bar{u}^{11/4}\, T}, \qquad (15a)$$

with

$$\bar{\lambda} = 0{,}316 \left(\frac{\bar{u}\, d}{\nu}\right)^{-1/4} \qquad (15b)$$

$\bar{\lambda}$ is a fictitious pipe resistance coefficient formed with the

temporal average $\bar{u}$. In order to apply these formulas, the law for $\bar{u}$ must be known with great accuracy, because the high power exponent $\bar{u}^{11/4}$ occurs, which will almost triple any small inaccuracy in $\bar{u}$ when $\bar{u}^{11/4}$ is formed. For an incompressible medium which is driven through a rigid pipe by means of a piston machine, we have positive controlled pulsations, which are specified by piston velocity and filling time. We find the machine flows* shown in Figures 23a-g. For each of them we have calculated

$$a = \frac{\int_0^T \bar{u}^{11/4}\, dt}{\bar{u}^{11/4}\, T}$$

which is given under each diagram. Figures 24 a and b show this quantity for the cases shown in Figures 23a and g. According to equation (15a), these must be multiplied by $\bar{\bar{\lambda}}$ in order to obtain the pipe resistance coefficient λ_p. /187

We would also like to state that Figures 23 a to g also show the variation of the flow velocity $\bar{u}$ as a function of time. The curves should be sinusoidal curves. In Figure 23a, s is the relative flow time [1]. This is the ratio of the time t_s, during which flow takes place to the pulsation duration T. Figure 23 g does not refer to any special machine flow. This is a constant basic flow superimposed on a pulsation having the relative amplitude γ. This is the ratio of the amplitude $\Delta\bar{u}$ to the temporal average value $\bar{\bar{u}}$ of the flow velocity.

8. SUMMARY

The flow and friction conditions in the unsteady, turbulent

(*) Other diagrams for machine flows see Ch. Schmidt, Measurement Errors for Flow Measurements of Pulsating Gas Flows, Z. VDI, Vol. 84, 1940, Nr. 33, p. 596-98.

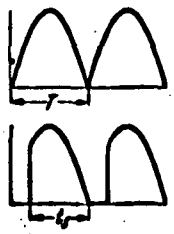

Figure 23a. Double acting piston compressor, t_s time duration of the mass flow; 100 $t_s/T=s$ [%]; calculation of ϵ as a function of s, according to Figure 24a.

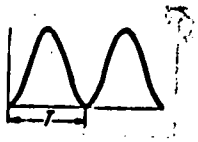

Figure 23b. Four cylinder four-stroke machine, $\epsilon=2.2$.

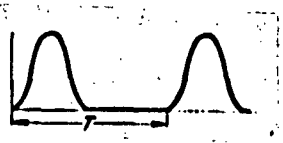

Figure 23c. Two cylinder four-stroke machine, $\epsilon=7.3$.

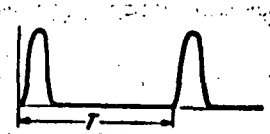

Figure 23d. One cylinder four-stroke machine, $\epsilon=24.8$.

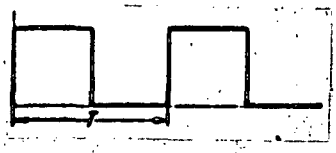

Figure 23e. $\epsilon=3.4$

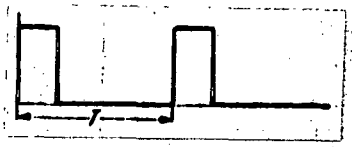

Figure 23f. $\epsilon=11.3$

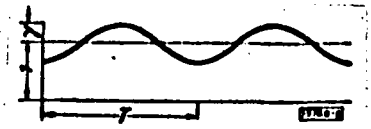

Figure 23g. Constant basic flow with superimposed pulsation. Calculation of ϵ according to Figure 24b.

Figure 23a to g. Assumed basic machine flows for determination of the pipe resistance for pulsation.

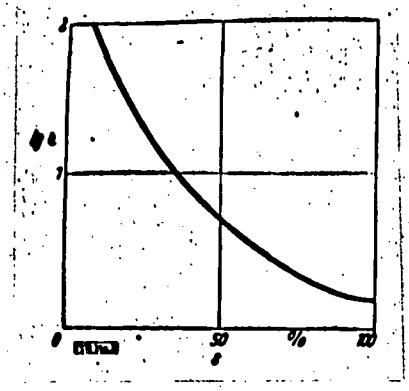

Figure 24a. Influence of the relative flow time s.

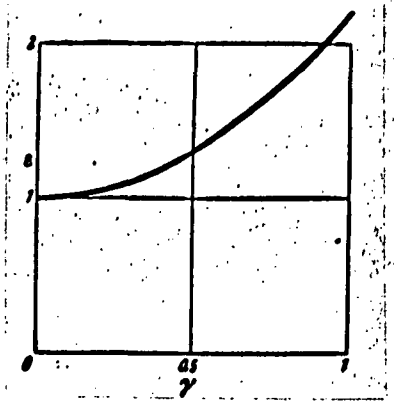

Figure 24b. Influence of the relative amplitude γ.

Figures 24a and b. Determination of the pipe resistance for pulsation.

friction layer were investigated for the case of pulsating pipe flow using pressure measurements carried out during the pulsations. Stagnation pressure measurements showed that there was reverse flow during the retardation period, which is similar to separation. This could also be demonstrated in flow visualizations.

The average pipe friction was determined using pressure decrease measurements and stagnation pressure measurements. Also we were able to determine the variation of the wall shear stress during one pulsation as well as the shear stress profiles at certain times. We derived the pulsation coefficients Ω ,Γ and the coefficients Ω', Γ' for the reverse flow in order to classify the experimental values with regard to reverse flow and pipe friction.

$$\Omega = \frac{\Delta \bar{u}}{T}\frac{d}{\bar{u}^2}, \qquad \Gamma = \Omega\,\mathrm{Re}^{1/4}, \qquad \Omega' = -\frac{d\bar{u}}{dt}\frac{d}{\bar{u}^2}, \qquad \Gamma' = \Omega'\,\mathrm{Re}^{1/4}.$$

We were able to show that the coefficients Ω', Γ' have the same meaning as those derived earlier by Prandtl for a diffusor.

The analogy between temporal and spatial retarded flow was very apparent from the shear stress profiles, which were influenced by temporal accelerations in the same direction as the influence of spatial accelerations.

In the range of small pulsation coefficients Γ we found that the steady state pipe friction law was approximately valid. Since it is known, it is possible to calculate the pipe resistance for pulsations within these limits. For this purpose we established the pipe resistance coefficient

$$\lambda_p = \frac{2d}{\varrho \bar{u}^2} \cdot \frac{\int_0^T \frac{dp}{dx} \bar{u}\, dt}{T \bar{u}}$$

which is a measure for the resistance power which must be expended. The pressure decrease dp/dx can be expressed by means of a steady state pipe friction law. Even though the pipe friction is not large, the pipe resistance is greater for pulsations. A resistance coefficient λ_p* found in the literature was found not to be appropriate and an increase in the pipe resistance by pulsations was found to be only produced by calculations because a quantity was averaged incorrectly. However this contradiction is removed if we use the quasi-steady case, i.e. the case of very long pulsation duration instead of the steady case, for which the steady state pipe friction law is exactly satisfied. As a practical application, we calculated the pipe resistance for a number of machine flows.

REFERENCES

1. Herning, F. and Chr. Schmid. Flow Measurements for Pulsating Flow, Z. VDI, Vol. 82, 1938, p. 1107-14, which also contains additional references.

2. Estel, E.. Flow Coefficient of Normalized Nozzles and Pressure Decrease in Pipes for Pulsating Flow, Phys. Z., Vol. 38, 1937, p. 748.

3. Nikuradse, J.. Gesetzmässigkeiten der Turbulenten Strömung in Glatten Rohren (Turbulent Flow Laws in Smooth Pipes), VDI-Forsch.-Heft 356, Berlin 1932.

4. Prandtl, L. New Results of Turbulance Research, Z. VDI, Vol. 77, 1933, p. 105-14.

5. Blasius, H.. The Similarity Law for Friction Processes in Liquids, VDI-Forsch, Heft 131, Berlin 1913.

6. Nikuradse, J.. Flow Laws in Rough Pipes, VDI-Forsch.-Heft 361, Berlin 1933.

7. Schultz-Grunow, F.. The Hydraulic Friction Resistance of Plates with Moderately Rough Surfaces, especially Ship Surfaces. Lecture at the 38th main meeting of Shipbuilder's Association, November 1937, J. Schiffbautechn. Ges., Vol. 39, 1938, p. 176-98.

8. Bauer, B. and F. Galavics. Experimental and Theoretical Investigations of Pipe Friction of Remote Hot Water Lines, Mitteilung aus Betrieb u. Forschung des Fernheizkraftwerks der Eidg. Techn. Hochschule, Zurich, 1936.

9. Nikuradse, J.. Investigations on Water Flow in Convergent and Divergent Channels, VDI-Forsch.-Heft 289, Berlin 1929.

10. Prandtl, L.. The Mechanics of Viscous Fluids, Contribution to F. Durand, Aerodynamic Theory, Berlin 1935, Vol. 3, p. 156.

Translated for National Aeronautics and Space Administration under contract No. NASw 2483, by SCITRAN, P. O. Box 5456, Santa Barbara, California, 93108.

STANDARD TITLE PAGE

1. Report No.	2. Government Accession No.	3. Recipient's Catalog No.
NASA TT F-14,881		

4. Title and Subtitle	5. Report Date
PULSATING FLOW THROUGH PIPES	April 26, 1973
	6. Performing Organization Code

7. Author(s)	8. Performing Organization Report No.
f. Schultz-Grunow	10. Work Unit No.
	11. Contract or Grant No. NASw-2483

9. Performing Organization Name and Address	13. Type of Report and Period Covered
SCITRAN Box 5456 Santa Barbara, CA 93108	Translation
12. Sponsoring Agency Name and Address National Aeronautics and Space Administration Washington, D.C. 20546	14. Sponsoring Agency Code

15. Supplementary Notes

Translation of: Pulsierender Durchflussdurch Rohre

Source: Forschung, Vol. 11, No. 4, 1940, pp. 170-187.

16. Abstract

Pulsating flow through pipes; test on straight pipe, flow through which is pulsating, to investigate instantaneous state of flow and friction of turbulent friction layer in case of non-stationary flow.

17. Key Words (Selected by Author(s))	18. Distribution Statement
	Unclassified - Unlimited

19. Security Classif. (of this report)	20. Security Classif. (of this page)	21. No. of Pages	22. Price
Unclassified	Unclassified	18	